Smooth Muscle and Skeletal Muscle Myosins Produce Similar Unitary Forces and Displacements in the Laser Trap

William H. Guilford,* Donald E. Dupuis,* Guy Kennedy,§ Junru Wu,# Joseph B. Patlak,* and David M. Warshaw*

Departments of *Molecular Physiology and Biophysics, and #Physics, and §Instrumentation and Modelling Facility, University of Vermont, Burlington, Vermont 05405 USA

ABSTRACT Purified smooth muscle myosin in the in vitro motility assay propels actin filaments at 1/10 the velocity, yet produces 3–4 times more force than skeletal muscle myosin. At the level of a single myosin molecule, these differences in force and actin filament velocity may be reflected in the size and duration of single motion and force-generating events, or in the kinetics of the cross-bridge cycle. Specifically, an increase in either unitary force or duty cycle may explain the enhanced force-generating capacity of smooth muscle myosin. Similarly, an increase in attached time or decrease in unitary displacement may explain the reduced actin filament velocity of smooth muscle myosin. To discriminate between these possibilities, we used a laser trap to measure unitary forces and displacements from single smooth and skeletal muscle myosin molecules. We analyzed our data using mean-variance analysis, which does not rely on scoring individual events by eye, and emphasizes periods in the data with constant properties. Both myosins demonstrated multiple but similar event populations with discrete peaks at approximately +11 and −11 nm in displacement, and 1.5 and 3.5 pN in force. Mean attached times for smooth muscle myosin were longer than for skeletal-muscle myosin. These results explain much of the difference in actin filament velocity between these myosins, and suggest that an increased duty cycle is responsible for the enhanced force-generating capacity of smooth over skeletal-muscle myosin.

INTRODUCTION

Smooth muscle contracts at 1/10 the unloaded shortening velocity of skeletal muscle (Fay et al., 1981). In addition, smooth muscle produces as much force per cross-sectional area of muscle as skeletal muscle with one-fifth the myosin, suggesting that smooth muscle myosin may generate higher force (Murphy et al., 1974). Indeed, these differences in muscle mechanics are paralleled at the level of the myosin molecule. In the in vitro motility assay, purified smooth muscle myosin propels actin filaments at 1/10 the velocity (v_{max}) of skeletal muscle myosins (Warshaw et al., 1990). Furthermore, smooth muscle myosin produces 3–4 times more time-averaged force (F_{avg}) than skeletal muscle myosin in an in vitro microneedle force-measurement assay (VanBuren et al., 1994b). However, these force and velocity comparisons were made from ensembles of 50–200 myosin molecules. Such measurements cannot discern differences in the magnitude and kinetics of force and displacement generated by individual smooth and skeletal muscle myosin molecules. This molecular comparison can, however, be accomplished by direct observation of the mechanical activity from single myosin molecules using the combination of the laser trap transducer and the in vitro motility assay. We report here such a direct comparison of unitary displacements, forces, and kinetics of smooth and skeletal muscle myosins.

The laser trap transducer uses a laser beam, focused to a diffraction-limited spot, to trap and hold translucent particles in solution (Ashkin et al., 1986). To observe unitary forces and displacements as myosin interacts with actin (Finer et al., 1994), an actin filament is strung between two independently trapped polystyrene microspheres and offered to purified myosin or (heavy meromyosin) HMM in an in vitro motility assay (Kron and Spudich, 1986; Harada et al., 1987). Forces and displacements generated by the myosin are transmitted through the actin filament to the trapped microspheres. The motion of one microsphere is taken as a measure of unitary displacements generated by the myosin. Alternatively, the position of the trap may be servo-controlled to hold the microsphere stationary. In this case, the position of the laser trap is taken as a measure of unitary forces generated by myosin.

Although the laser trap measurements from single myosin molecules are powerful, the interpretation of data from such experiments is not straightforward. At the trapping strengths that must be used, the Brownian motion of the microspheres is on the same order of magnitude as the displacement in a myosin-actin interaction. Furthermore, a range of different step sizes is observed, including steps in the reverse of the predominant direction of movement. Quantification of such complex activity will thus be critical to its interpretation. Different investigators have reported values of the unitary displacement step in skeletal muscle HMM that range from 4 nm (Molloy et al., 1995a) to 35 nm (Miyata et al., 1994), depending on the model used to analyze and interpret the data.

Received for publication 26 December 1995 and in final form 20 November 1996.

Address reprint requests to Dr. David M. Warshaw, Department of Molecular Physiology and Biophysics, University of Vermont, Given Medical Building, Room D-205, Burlington, VT 05405-0068. Tel.: 802-656-4300; Fax: 802-656-0747; E-mail: warshaw@salus.med.uvm.edu.

0006-3495/97/03/1006/16 $2.00

The challenges imposed by laser trap data are similar in many respects to those encountered in the analysis of data from single ion channels, where currents switch rapidly between two or more amplitudes in records contaminated by significant background noise. In both analyses it is desirable to measure, in a model-independent manner, the distribution and duration of event sizes. One method, derived originally for use in channel data (Patlak, 1993), is called "mean-variance analysis." It transforms the temporal data sequence into a three-dimensional histogram that emphasizes intervals in the data with steady properties. The mean-variance transform condenses the data in a model-independent way for subsequent qualitative and quantitative interpretation.

We use this method of analysis to help provide us with an objective measurement of the motion and force from single skeletal and smooth myosin molecules. We find that smooth and skeletal muscle myosins produce similar unitary displacements, but that smooth muscle myosin has fourfold longer attachment times, helping to explain the differences in velocity for these two myosin types. In addition, smooth and skeletal muscle myosins produce similar unitary forces (F), suggesting that smooth muscle myosin's enhanced average force generation compared to skeletal muscle myosin (Harris et al., 1994; VanBuren et al., 1994b) is most likely due to a difference in the kinetics of the cross-bridge cycle for these myosins. Finally, because of the novelty of the laser trap in making these measurements, we have dedicated significant discussion to possible sources of error in determining myosin's unitary displacement (d) and have outlined approaches to minimizing the contribution of these errors to estimates of d.

MATERIALS AND METHODS

Proteins

Smooth (turkey gizzard) and skeletal (chicken pectoralis) muscle myosins were prepared as previously described (Warshaw et al., 1990). Smooth-muscle myosin was thiophosphorylated by incubation with light-chain kinase, calmodulin, 1.5 mM $CaCl_2$, and adenosine 5′-γ-(thiotriphosphate). Monomeric myosin was stored at −20°C in 50% glycerol.

Actin was isolated from chicken pectoralis acetone powder as previously described (Pardee and Spudich, 1982) and stored as filaments at 4°C. Previous studies confirmed that smooth and skeletal muscle isoforms of actin are functionally identical in the in vitro motility assay (Harris and Warshaw, 1993b); therefore all measurements were performed with skeletal muscle actin. Actin was fluorescently labeled by incubation with tetramethylrhodamine isothiocyanate (TRITC)-labeled phalloidin (Sigma) for at least 2 days before use (Warshaw et al., 1990).

In vitro motility assay

Solutions for the in vitro motility assay were prepared as previously described (Warshaw et al., 1990). All experiments were performed at limiting MgATP concentrations (10 μM). Using this MgATP concentration increased unitary event durations and thus improved our ability to resolve these events.

Solution concentrations were as follows. Myosin buffer: 300 mM KCl, 25 mM imidazole, 1 mM EGTA, 4 mM $MgCl_2$, 10 mM dithiothreitol, pH 7.4. Actin buffer: 25 mM KCl, 25 mM imidazole, 1 mM EGTA, 4 mM $MgCl_2$, 10 mM dithiothreitol, 10 μM MgATP, pH 7.4, oxygen scavenger system (0.1 mg/ml glucose oxidase, 0.018 mg/ml catalase, 2.3 mg/ml glucose).

Flow cells were constructed of two nitrocellulose-coated, 25-mm-square, no. 1 glass coverslips, separated by 1.5 mil (~38 μm), immersion oil-dipped, mylar shim stock (McMaster Carr). This arrangement formed a 15-μl experimental chamber. On one of the two coverslips, we used glass beads to create "pedestals" to position myosin molecules off the surface of the coverslip (Finer et al., 1994). Briefly, 0.4 mg/ml of 2-μm glass beads (Bangs) were suspended by sonication in methanol, applied to glass coverslips with a thin-layer chromatography sprayer, and allowed to dry. Nitrocellulose was then applied over the beads and onto the coverslip as previously described (Warshaw et al., 1990).

NEM beads

N-Ethylmaleimide (NEM)-modified myosin is a strong binding analog that does not hydrolyze MgATP, and therefore was used to irreversibly bind actin to our microspheres. NEM-myosin was prepared as previously described (Warshaw et al., 1990) and bound to latex microspheres by the following protocol.

Polystyrene microspheres (1 μm, ~2 × 10^8) with primary amino surface groups (Polysciences) were suspended in 50 μl of NEM-myosin (~4 mg/ml in 50% glycerol) by vigorous sonication and incubated at room temperature for 15–30 min. TRITC-labeled ovalbumin (200 μl, 0.05 mg/ml; Sigma) in myosin buffer was added to the suspension and incubated for an additional 1–2 min. Finally, the microspheres were washed once and resuspended in actin buffer. Microspheres were prepared daily.

The laser light trap

In Fig. 1 *a* is a simplified schematic representation of the laser light trap instrument, the technical details of which have been described previously (Dupuis et al., 1997). In brief, the beam of a variable-power Nd:YLF TFR solid-state laser (3 W, 1047 nm; Spectra Physics) was split into two orthogonally polarized beams. Each beam was expanded by an independent telescope to fill the back-aperture of a microscope objective (100×, n.a. 1.4; Nikon). The position of each trap was coarsely controlled by translating the first lens (Fig. 1 *a*, L) forming the telescope. The beams were recombined by a cubic beamsplitter before entering the microscope objective, which focused the beams to form two independent optical traps.

The microscope (Lab Standard, Zeiss) was equipped with brightfield and epifluorescence illumination. The experimental flow cell chamber was placed on the microscope stage and oil coupled to both the objective and the condenser (n.a. 1.4). The temperatures of both the objective and condenser were controlled to maintain the flow cell at 25°C. The entire stage was insulated against temperature fluctuations.

The brightfield image of one of the trapped microspheres was projected onto a four-quadrant photodiode detector (Fig. 1 *a*, QD; UDT Sensors). Two QD output signals indicated the microsphere's position along x and y axes with nanometer resolution. These signals were stored on videotape with a recording adapter (model 3000A; Vetter) for later analysis. The bandwidth of the QD was in excess of 9 kHz. However, biological data were filtered such that the overall frequency response rolled off slowly, beginning at ~1–2 kHz (see Fig. 1 *b*). The recorded data were later digitized at 2.5 kHz, using a 2801A A/D board and Global Lab computer software (Data Translation). Force and displacement data were routinely recorded both parallel and perpendicular to the actin filament (i.e., QD x and y axis, respectively).

Measurement of isometric force

Isometric force was measured as described previously (Finer et al., 1994; Simmons et al., 1996). Briefly, the position of one of the traps is controlled with an acousto-optic modulator (AOM) (NEOS). The signal from the QD enters a feedback network, which in turn controls the AOM. Using feed-

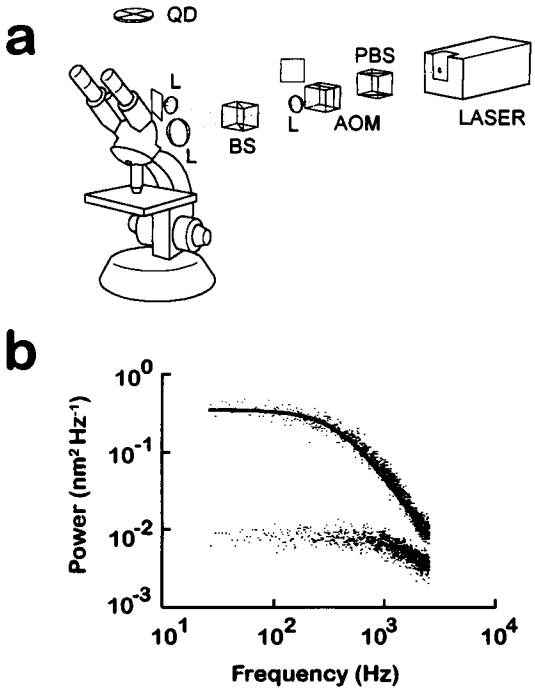

FIGURE 1 (*a*) Schematic diagram of the laser trap used in these studies. PBS, Polarizing beam splitter; BS, beam splitter (recombining); L lenses forming the telescopes; QD, quadrant detector; AOM, acousto-optic modulator. (*b*) Power density spectrum of the motion of a microsphere captured in the optical trap (*upper trace*) and the brightfield noise (*lower trace*). The brightfield noise is provided as an indication of signal-to-noise ratio. The actual detector bandwidth was 9.4 kHz, as determined by shining a white-noise light source directly onto the quadrant detector (data not shown). The line shows the best fit of Eq. 2, giving a corner frequency of 530 Hz, once corrected for inline filtering (2 kHz). This results in a trap stiffness of 0.031 pN/nm for this example; equipartition theory (Eq. 1) predicts a similar value of 0.034 pN/nm.

back control, one microsphere is held stationary by rapidly deflecting the trap with the AOM. Isometric force is measured as a linear function of trap displacement, because the trap behaves as a linear spring over short displacements from the center. The closed-loop bandwidth of the force transducer was ~400 Hz. However, microsphere position was poorly controlled at frequencies above 140 Hz.

Trap stiffness

Trap stiffness (α_{trap}) was routinely obtained by the equipartition method, as described previously (Svoboda and Block, 1994). α_{trap} was calculated from Boltzman's constant (k_B), the absolute temperature of the fluid medium (T), and the variance of the trapped microsphere's Brownian motion (σ^2):

$$\alpha_{trap} = k_B T/\sigma^2. \quad (1)$$

As an independent measure, trap stiffness was obtained from the "corner frequency" of the thermal motion of the microsphere (Svoboda and Block, 1994). Briefly, the motion of the microsphere in the trap was recorded and the power density spectrum (PDS) calculated by standard methods (Press et al., 1988) (see Fig. 1 *b*). We fit the PDS with a Lorentzian of the form

$$k/(f^2 + f_0^2), \quad (2)$$

where f_0 is the corner frequency, and k is a lumped parameter that includes viscous drag (β) on the microsphere. α_{trap} is related to f_0 by

$$f_0 = \alpha_{trap}/(2\pi\beta). \quad (3)$$

When estimating corner frequencies, one must consider not only the dynamics of the microsphere, but the frequency response of the entire system, including the detector, and any additional filters. Each component can be treated as an independent "filter" with its own corner frequency. Thus the true corner frequency of the microsphere must be corrected for the effects of series filtering. Assuming the microsphere and the electronics to be "matched" filters (i.e., of similar roll-off properties), we estimated the true corner frequency of the microsphere, f_0, from the equation

$$1/f_m = 1/f_0 + 1/f_e, \quad (4)$$

where f_m is the measured corner frequency of the microsphere, and f_e is a lumped parameter describing the corner frequency of all the external electronics. The importance of applying this correction cannot be overstated. For example, to measure the true corner frequency to within 10% error, one would need a lumped system bandwidth of at least $9 \times f_0$, even though there is little Brownian motion remaining above $2 \times f_0$. However, filtering and correction with Eq. 4 give results that are consistent with other measures of trap stiffness (Dupuis et al., 1997; and Fig. 1). Typically, stiffness of a single trap in our experiments was 0.03–0.04 pN/nm.

Experimental protocol

Before the experiment, inactive myosin was removed from solution by mixing myosin (250 μg/ml) in myosin buffer with an equimolar quantity of filamentous actin and 1 mM MgATP. The solution was spun (AirFuge) for 20 min to pellet the actin and attached inactive myosin. The supernatant was diluted with myosin buffer to a final myosin concentration of 5 μg/ml. TRITC-phalloidin-labeled actin (0.03 mg/ml) was diluted approximately 200-fold in actin buffer just before use.

Solutions were applied to the flow cell in 15 μl aliquots in the following order: 1) myosin (5 μg/ml) in myosin buffer for 20 s, 2) 0.5 mg/ml bovine serum albumin (Sigma) in myosin buffer for 30 s, and 3) two washes of actin buffer. Finally, equal volumes of NEM-myosin microspheres and labeled actin (both in actin buffer with 10 μ M MgATP) were mixed and immediately introduced to the flow cell. The flow cell was quickly transferred to the microscope to minimize the time available for the microspheres to adhere to the coverslip surfaces.

A microsphere was captured in each of the two laser traps, and an actin filament was strung between them (Fig. 2). One of the microspheres was carefully centered on the QD, and the other was adjusted to preload the actin filament to ~2–4 pN. Adequate pretensioning of the actin filament was necessary to reduce an effective compliance that results from the manner in which the actin is attached to the microsphere (Dupuis et al., 1997). The actin filament was centered over a 2-μm glass bead on the motility surface, and lowered (using a 10:1 geared-down fine focus) until force or displacement events were observed. When necessary, we arranged the actin filament polarity by manipulating the traps such that "forward" displacements (distinguished by the predominant direction of events) pulled the microsphere being observed further away from the trap center, thus adding additional tension to the filament (Finer et al., 1994; Dupuis et al., 1997). Data were discarded if we observed significant displacements or forces perpendicular to the actin filament.

The QD sensitivity and trap stiffness (see above) were determined after each measurement, generally using the same microsphere from which the biological measurements were made. The actin filament was slackened, and the QD voltage sensitivity was obtained by moving the microsphere in a series of 7.7-nm steps with the AOM.

ANALYSIS

The step displacements caused by myosin are on roughly the same scale as the microsphere's Brownian motion.

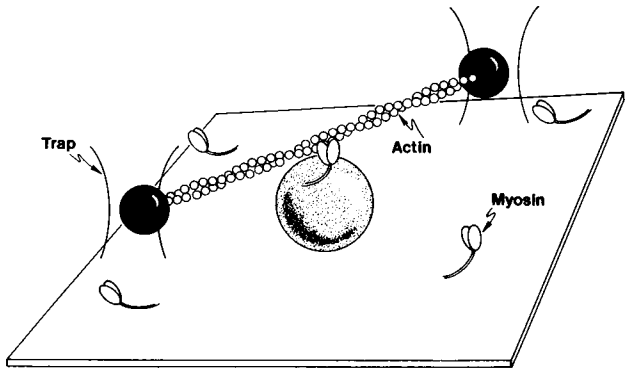

FIGURE 2 An illustration of the use of the laser trap to study force and displacement in the in vitro motility assay. Two microspheres are captured in independent light traps (*dark spheres*), and an actin filament is held taut between them. A coverslip with scattered silica microspheres (*speckled sphere*) is sparsely coated with myosin. The coverslip is moved toward the traps until myosin interacts with the actin filament, and unitary force or displacement events are observed from one of the trapped microspheres.

Thus, identifying and measuring displacement and force events was difficult.

Previously, Finer et al. (1994) identified events by eye and subjected them to several criteria for acceptable data. In a more recent study, Molloy et al. (1995a) identified events by looking for reductions in Brownian motion of the trapped microsphere that accompanied periods of cross-bridge attachment to actin. In both studies, however, events were hand-selected. Hand selection could significantly bias the data, and it is a difficult practice to defend statistically (Block and Svoboda, 1995).

To derive an unprejudiced estimate of force and displacement from our data, we used the technique of "mean-variance" (MV) analysis (Patlak, 1993), originally developed for the statistical analysis of single ion-channel current data. Like ion channel recordings, single time records of displacement or force events produced by myosin appear as "steps" in the data record, and are thus amenable to this style of analysis, which emphasizes and allows the investigator to identify intervals of constant amplitude within the data.

The basis of the technique is to transform data into a mean-variance histogram. Thus, MV analysis begins with a model-independent transformation of the data, giving an alternative view of the data. Quantitative and statistical descriptions of the data are subsequently derived from curve fits to the transformed data. Although such measurements may depend upon assumptions about the form of the underlying data, they are less prone to the biases introduced by manual scoring methods.

Our description of MV analysis is designed to brief readers who are not familiar with the application of this technique to single channels. We will therefore describe the technique and its application to measuring unitary displacements in three sections: 1) the MV transform and histogram generation; 2) general principles of interpretation and derivation of meaningful statistical parameters from MV histograms; and 3) specialized procedures we employed in applying MV analysis to data obtained with the laser trap. For additional information on this technique, we refer the reader to Patlak (1993).

Generating the mean-variance histogram

The mean-variance transform associates a mean and variance estimate with each sample point in a data record (Fig. 3). These mean/variance estimates are from the N data points including and immediately preceding the sample, where N is called the "window width." The MV estimates can be kept as a time sequence, or they can be assembled into a three-dimensional histogram of binned mean versus log-binned variance. This latter form is called the mean-variance histogram. The third axis of the MV histogram is the total number of sample points (i.e., cumulative time) spent at a particular mean and variance.

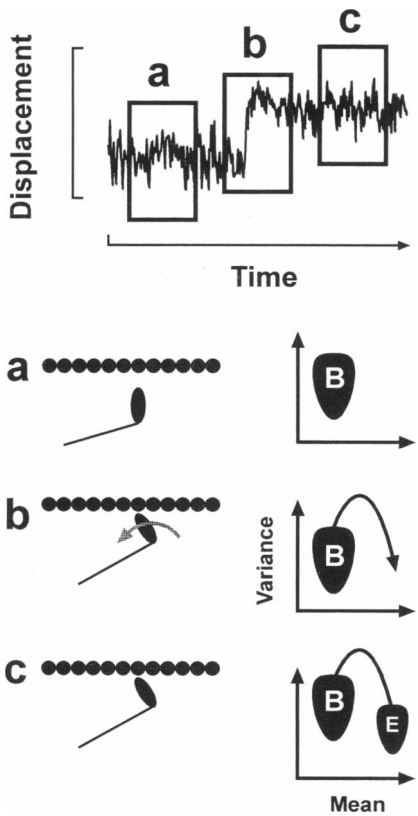

FIGURE 3 An illustration of mean-variance (MV) analysis on a single step (*top*). A window is moved across the data (*boxes*) from left to right. The bottom three panels show the MV histogram as it develops, moving through (*a*) baseline, and (*b*) the transition to (*c*) a plateau in the data. These three states are thought to correspond to periods when myosin is (*a*) detached from actin, (*b*) going through a power stroke, and (*c*) strongly bound to actin. Notice that unchanging areas in the data (baseline and plateau) appear as populations (B and E, respectively), whereas the transitional region appears as an "arch" that can be excluded from analysis. Myosin lends its stiffness to the actin and beads when attached, thus events (E) are also distinguished from baseline (B) by their lower variance.

Generation of the MV histogram requires no assumptions about or interpretation of the underlying data. However, certain common features of the resulting histogram derive directly from common statistical elements in the data. The histogram tends to emphasize periods in which the sampled data are constant for at least the duration of the window. Such intervals will be devoid of any additional variance due to the inclusion of transitions between different levels. Fig. 3 illustrates the process of assembling mean and variance estimates into an MV histogram.

When the original record contains a noisy background, such as the microsphere's Brownian motion, the MV histogram will show a characteristic region, centered on a mean of zero (i.e., baseline), that describes the statistical properties of this background noise (see Fig. 3 *a*). However, when other transiently steady levels or steps are found within the record (for example, the period of myosin attachment), additional regions will appear in the MV histogram that are centered on the mean value for their respective levels (Fig. 3 *c*). These additional regions may not have a distribution of variance estimates similar to that of the baseline. In fact, the previously described reduction in microsphere position variance that accompanies the attachment of myosin to actin in the laser trap (Finer et al., 1994; Molloy et al., 1995a) becomes a useful tool for separating unitary events from baseline noise (see Results).

Interpretation of MV histograms

The third dimension of the MV histogram describes the number of entries (the total time spent) at a given mean variance (Fig. 4 *a*). Thus each discrete region of the MV histogram will describe a probability density for being at a given level at any point in time. When such intervals are frequent, the region associated with this level in the MV histogram will have a high probability density or "volume" and will appear as a "peak" in the histogram (see Fig. 4). Therefore, a given population of events with a high probability of occurrence can be identified within the MV histogram as a discrete region, characterized by its mean level, and associated variance. The "noise" in the data during events or baseline is reflected in the position of a population on the variance axis. The "width" of a population on the means axis is a reflection of the inherent variability of an event or baseline population, not the noise during events or baseline. Patlak (1993) showed further that the total amount of time spent in a given population, when measured as a function of window width, can be used to measure the mean on-time for the population (see below), assuming the events are stochastic and exponentially distributed.

Two strategies can be used in the interpretation of the MV histogram. The first would be to propose a model that is capable of replicating the observed MV histogram at a set of window widths. The second strategy does not require a model, but rather associates the histogram peaks with discrete components or populations within the data record (e.g., baseline, steady displacements of amplitude *d*, etc.) and then characterizes these components separately based on their amplitude, relative frequency, and duration. We use both strategies here.

Fitting components of the MV histogram

Individual components or regions of the MV histogram must be fitted to determine their relevant parameters (i.e., population mean, variance, and volume). Because each component is described by a three-dimensional peak, fitting of this peak can be approximated by the product of the population's probability density in the mean dimension with its probability density in the variance dimension (see Fig. 4, *b* and *c*), as originally adopted in Patlak (1993).

In the mean dimension, the histogram is generally composed of the sum of Gaussians, each spread with a standard deviation related to the variability of the data and to the window width, N (the number of samples encompassed by the window).[1] These were fit by a standard Levenburg-Marquardt minimization (Press et al., 1988), once the data were "rebinned" to eliminate bins with zero counts. Similarly, the variance associated with each mean will also spread about its true value because of the statistical uncertainty of determining this variance from a series of estimates, each based on a finite number of points, N. In the variance dimension, the histogram can be described by a χ^2 function, which was fit using a Simplex algorithm (Press et al., 1988) to provide estimates of the population variance (σ^2) and the degrees of freedom (i.e., the inverse "width" of the χ^2 distribution). These separate distributions are most accurately characterized when the mean distribution is estimated from a histogram cross section taken at the population variance, and the variance distribution is estimated at the peak mean value for each component. These optimal values are determined by iterative fits.

Separating event components from baseline

The ability to characterize individual components within the MV histogram as described above assumes that these components or populations are distinctly separate within the histogram. This condition assumes that, for any component, its variance distribution contains entries from only that component. However, this condition is not necessarily met in our biological data, where the baseline population in the MV histogram might overlap in variance with the popula-

[1]The distribution of mean values derived from 10 or more individual estimates is almost always well approximated by a single Gaussian. Therefore, mean entries into a MV histogram will have a Gaussian distribution any time the underlying process has a steady "population" mean value. If, however, there is an underlying probability density $P(x)$ favoring events of certain sizes, then observed event populations will be distributed as the convolution of $P(x)$ and one or more Gaussians. Any reasonable probability density function could, in principle, be fit to the data, although herein they were assumed to be the sum of a small number of Gaussians.

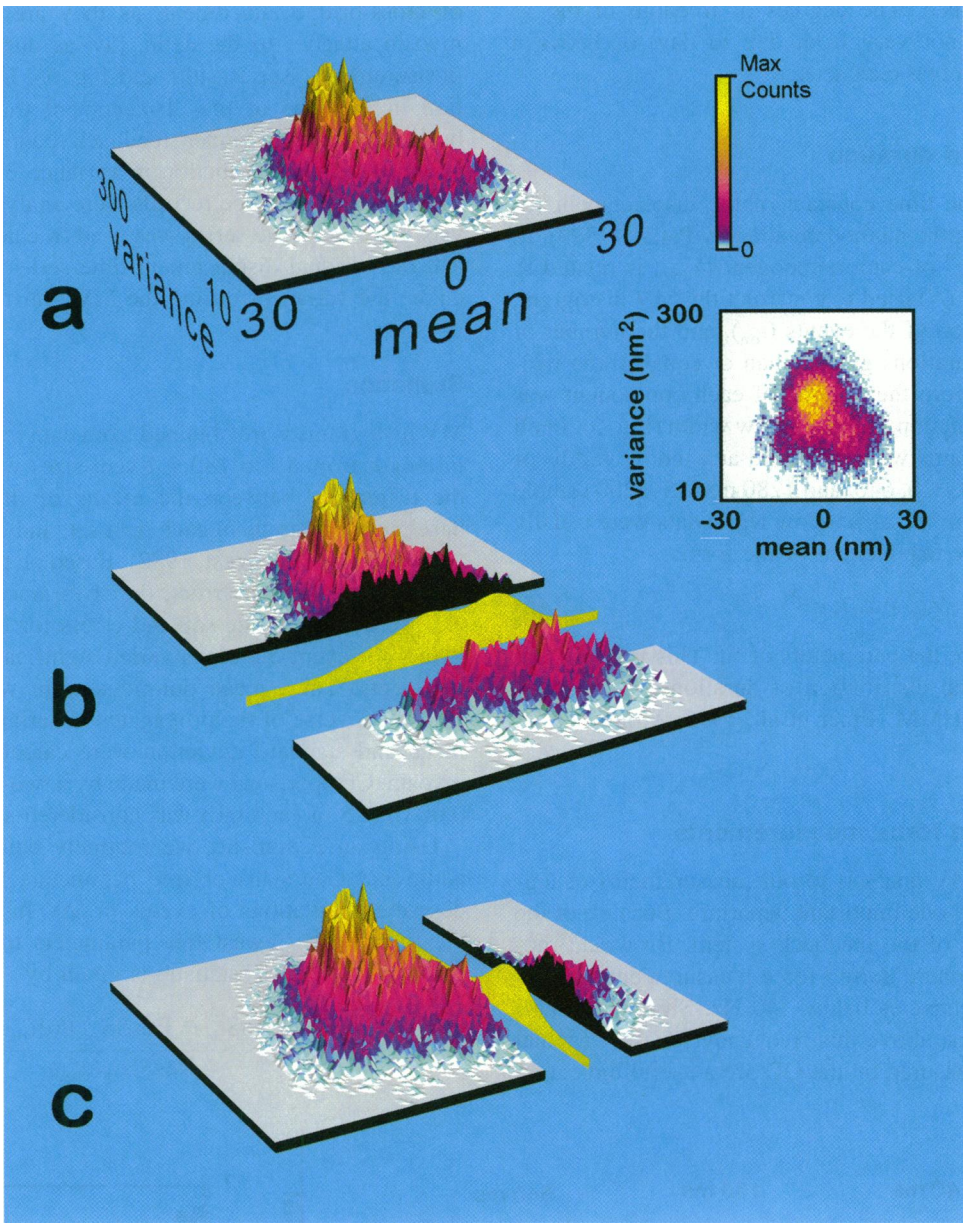

FIGURE 4 An example of mean-variance (MV) analysis and curve fitting on a skeletal muscle myosin displacement record. (*a*) the raw MV histogram of the data set (20-ms window). The number of counts in each bin is coded both by height and by color (see color scale). The maximum count in this histogram is 161, which corresponds to a cumulative time of 64 ms at that particular mean and variance. The same histogram is also shown as a two-dimensional projection (*inset*), which is the form used throughout the remainder of this text. In addition to the large, central peak representing the baseline, notice the populations that appear to extend into the low-variance region of the histogram. This is more easily visualized in the two-dimensional projection. Forward events lie to the right (positive displacements), and reverse events lie to the left (negative displacements). (*b*) The histogram has been divided at the level of the population variance for the events. Peaks representing baseline and forward events are evident. The less numerous reverse events are more difficult to discern. This profile was fit with three Gaussians (*yellow section*). (*c*) A section through the forward events at the level of their population mean was fit with a χ^2 (*yellow section*).

tion of myosin displacement events (see Fig. 4 *b*). To obtain accurate estimates of the event population parameters, it is imperative that the baseline MV component be separately determined in the absence of myosin activity and then subtracted from the MV histogram obtained in the presence of unitary events. This approach avoids errors that could arise from direct characterization of the baseline population in the presence of myosin activity. Failure to do so will often result in unwanted "removal" of events near zero displacement. Therefore, we routinely predetermined the "degrees of freedom" of the χ^2 distribution, from either myosin-less data sets or data collected just before contact with the motility surface, with the traps at virtually the same height above the coverslip as during actual recordings. This parameter was held fixed in subsequent fits of baseline populations, while the amplitude and population variance

were not constrained. The degrees of freedom of the χ^2 distribution does not vary from day to day, or between myosin-less and actual data sets.

Measuring event duration

We determined the time constant of the displacement (or force) events using the method detailed by Patlak (1993). In brief, the "volume" of each component (V_{mv}) is related to the window width (N) used to construct the MV histogram, the average duration of the events (t_{on}), and the number of events (κ) with durations greater than or equal to the window width. Therefore the volume of each component was determined as a function of the window width (Fig. 5). In all cases, MV histograms were produced at window widths of 10, 20, 40, 80, 160, 320, 640, and 1280 ms (25–3200 sample points). The volume versus window width data were usually well fit by a single exponential of the form:

$$V_{mv} = t_{on}\kappa\, e^{-(N-1)/t_{on}}, \quad (5)$$

where κ and t_{on} are the parameters of fit. This is consistent with an exponential distribution of durations observed by others in skeletal HMM (Finer et al., 1995; Molloy et al., 1995b).

MV analysis and force measurements

We also applied MV analysis to our measurements of unitary force, but with one important departure. Because of the limited bandwidth of the feedback system, Brownian motion of the microsphere during force measurements is only suppressed at frequencies below 140 Hz. Significant thermal motion remains above this frequency. These "residual displacements" measured by the QD are a useful indication of cross-bridge attachment, as they are reduced when a myosin attaches to the actin, just as during displacement measurements (see Results and Fig. 7). Indeed, the reduction in variance of the displacement trace during cross-bridge attachment under feedback control is more pronounced than the reduction in variance of the force trace. Therefore, when force records were analyzed by MV analysis, the force time series was used to calculate the means, and the residual displacement time series was used to calculate the variances during the MV transformation.

Statistics

MV histograms were obtained from data records that ranged in length from 10 to 180 s. Event sizes were calculated as the difference between the means of the event and the baseline populations in each data set, and errors were propagated (Skoog and West, 1982). Based on the assumption of normally distributed errors, the covariances of fit parameters were taken as the squared errors for those parameters. Errors for event durations varied significantly between experiments. Thus, mean durations were weighted by $1/\sigma^2$ (i.e., the inverse of the propagated covariance) when a final mean and standard deviation were calculated for a given myosin. Comparisons were made by a two-tailed Z test. $p < 0.05$ (0.025 in each tail) was considered significant.

Using an F statistic, we routinely determined whether additional Gaussians or free parameters were required to describe populations of events in MV histograms. Taking the fit with the fewest free parameters to be the null hypothesis (H_0), the F statistic is given by

$$R = \frac{(\mathrm{ResSS_{H_0}} - \mathrm{ResSS_{Alt}})/(\mathrm{df_{H_0}} - \mathrm{df_{alt}})}{\mathrm{ResSS_{Alt}}/\mathrm{df_{Alt}}}, \quad (6)$$

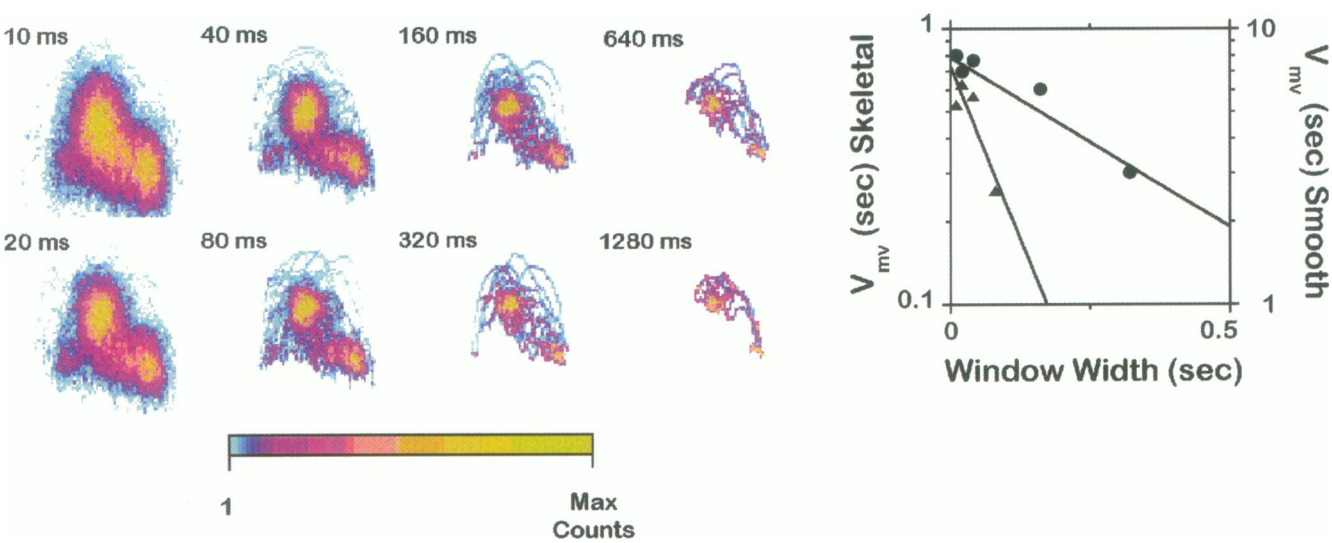

FIGURE 5 MV histograms of a smooth muscle myosin displacement record generated by using differing window widths (10–1280 ms). Increasing window widths emphasize events of greater duration. The graph at right shows the "volume" of forward events for both a smooth (●) and a skeletal (▲) data set. Lines represent a fit of Eq. 5 to the data. The fit parameters of Eq. 5 are the mean attached time (t_{on}) and the number of events (κ).

where $ResSS_x$ denotes the residual sum of squares for the fit, df_x is the degrees of freedom for the fit (reduced by the number of free parameters), and the subscripts H_0 and Alt specify the null and alternative, respectively. $p < 0.01$ was considered significant.

RESULTS

Unitary displacements

Examples of displacement records from smooth and skeletal muscle myosins are shown in Fig. 6. Typically, the data contain considerable periods of baseline noise interspersed with both "forward" and "reverse" or backward-directed displacements, as observed by others (Molloy et al., 1995a,b). When sufficiently high concentrations of either myosin (>20 μg/ml) were used, "ramps" or multiple events that cause a steady displacement of the microsphere away from the center of the trap were observed (data not shown). Such data were not included in this analysis. By inspection, the most notable difference between the two myosins is that smooth muscle myosin appears to have longer event durations than skeletal muscle myosin.

When the displacement records were transformed into MV histograms, a characteristic appearance was obtained for both smooth and skeletal muscle myosin (Fig. 6). The MV histogram contained several regions, the most obvious being a large central region with high variance associated with the Brownian motion of the trapped microsphere. This is the result of periods when myosin is detached from actin, as confirmed by comparison to MV histograms obtained in the absence of myosin. A G-test goodness of fit estimator indicated that the histogram for this region along the mean axis at the level of the population variance was well fitted by a single Gaussian. Note that the population variance of this region translates (see Eq. 1) into a system stiffness (~0.06–0.08 pN/nm) equal to twice that of a single trap, suggesting that the two microspheres are linked effectively by a rigid structure (Dupuis et al., 1997).

To either side of the baseline histogram, event populations were clearly discernible (Fig. 6, right). These popula-

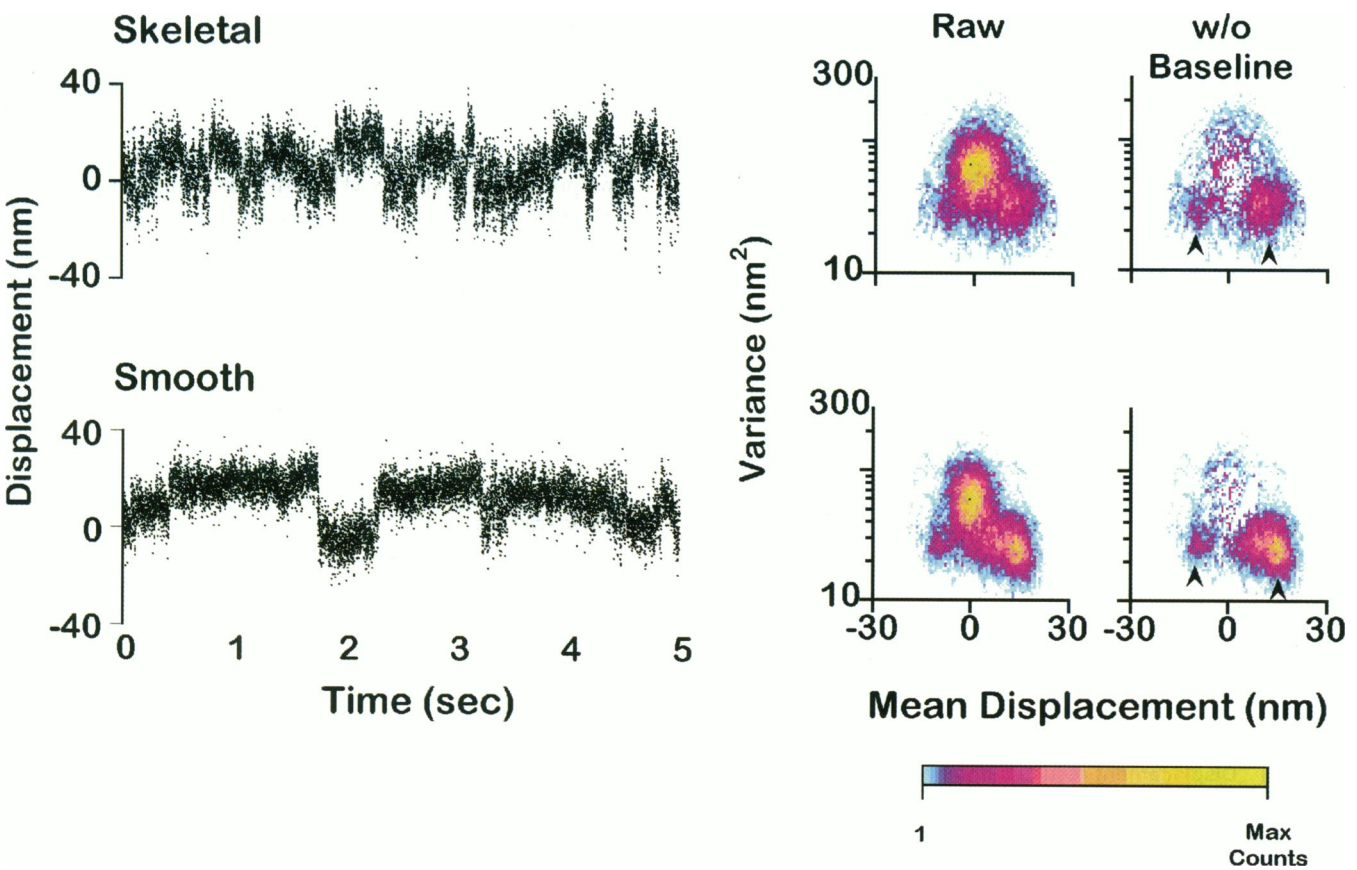

FIGURE 6 Example raw displacement data (*left*) and corresponding raw and baseline-subtracted MV histograms (*right*) for entire smooth and skeletal muscle myosin data records (30 s in skeletal, and 37 s in smooth; 20-ms window). Discrete forward and reverse event populations are evident in both myosins (*arrows*). The maximum count is 161 (64 ms) in skeletal, and 269 (107 ms) in smooth muscle myosin histograms. Parameters of fit for the forward event population in the pictured skeletal muscle myosin histogram: population mean ± covariance, 9.84 ± 0.05 nm; standard deviation ± covariance, 5.04 ± 0.03 nm; population variance, 33.5 nm^2; degrees of freedom, 27. Parameters of fit for the forward event population in the pictured smooth muscle myosin histogram: population mean ± covariance, 9.95 ± 0.01 nm; standard deviation ± covariance, 4.46 ± 0.01 nm; population variance, 29.2 nm^2; degrees of freedom, 26.

tions were distinguished from the baseline by both their means and their reduced population variance. As others have shown, the variance in the microsphere position trace is decreased during displacement events (Finer et al., 1994; Molloy et al., 1995a), presumably because of the increase in system stiffness that would accompany cross-bridge attachment (see Eq. 1 and Block, 1995).

To characterize these populations accurately, the baseline contribution was subtracted as described in Materials and Methods, leaving only the event populations and histogram entries due to transitions between levels (Fig. 3 *b*). When curve fitting to these data, we did not constrain the fits to a predetermined number of components. Even if two populations of events appeared to be present, these data were first fitted to one broadly distributed population (i.e., a single Gaussian, as suggested by Molloy et al., 1995a) and secondly to multiple unconstrained Gaussians. The condition that best fitted the data was determined by the F statistic (Eq. 6), as described in Materials and Methods. In 11 of 13 separate experiments for both smooth and skeletal muscle myosin, a single broad Gaussian did not adequately describe the data, suggesting the presence of one or more distinct populations (e.g., forward and reverse populations). The number of events analyzed for smooth and skeletal muscle myosins was on the order of 10^2 and 10^3 events, respectively.

When the majority of experiments that contained multiple event populations were analyzed, smooth and skeletal muscle myosins demonstrated similar mean forward displacements of 10.7 and 10.6 nm, respectively (Table 1). These displacement values are comparable to those reported by Finer et al. (1994) but twice that of Molloy et al. (1995a) for skeletal muscle HMM. Reverse events were not significantly different in magnitude from forward events (Table 1). However, in skeletal and smooth muscle myosins, respectively, forward events were approximately 2.6- and 4.5-fold more probable to occur than reverse events. We occasionally observed an additional small population of events at approximately 22 nm (twice the principal population) or at 0 nm. It is important to note that measured displacements will be attenuated because of series compliance in the system (see Materials and Methods).

As mentioned above, 11 of 13 experiments were best described by discrete event populations. However, two data sets from skeletal muscle myosin were adequately described by the single, broad distribution predicted by Molloy et al. (1995a). Specifically, a single population of events was evident and was adequately fit by a single Gaussian constrained to

$$\sigma = (\sigma^2_{\text{baseline}})^{1/2}, \tag{7}$$

where $\sigma^2_{\text{baseline}}$ is the variance of the baseline population in that particular data set, and σ is the standard deviation of the event population. The estimated unitary displacement for these two data sets was 6.1 ± 1.0 nm. This value is close to the ~4 nm predicted for skeletal muscle S-1 (Molloy et al., 1995a).

As mentioned above, event durations for smooth muscle myosin appear qualitatively longer than for skeletal myosin. To quantify these durations we constructed MV histograms at multiple window widths and plotted volume versus window width (Fig. 5), as indicated in Materials and Methods. The results of this analysis are given in Table 1. Smooth muscle myosin unitary displacements, both forward and reverse, were approximately 4 times longer in duration (t_{on}) than those observed in skeletal muscle myosin. The mean value of 44.9 ms for skeletal muscle myosin forward events was similar to the values previously reported for skeletal muscle HMM (Finer et al., 1994; Molloy et al., 1995a). Interestingly, forward events were longer in duration than reverse events, although this difference was statistically significant only in skeletal muscle myosin. This is in contrast to the results of Molloy et al. (1995a), who found durations to be independent of displacement direction.

The presentation of the MV histograms at multiple window widths also serves to emphasize the distinct nature of the event populations. At short window widths, the various regions are considerably wider in all dimensions as compared to histograms at longer window widths. This difference is due to the fact that MV histograms begin to converge on the true population means and variances at longer window widths as the contribution of noise in the data is averaged out.

Unitary forces

Examples of unitary force measurements for smooth muscle and skeletal muscle myosins are shown in Fig. 7. These data are similar in character to the displacement records in which both positive and negative force events were observed,

TABLE 1 Displacement results summary

	d (nm)		t_{on} (ms)	
	Forward	Reverse	Forward	Reverse
Skeletal	10.6 ± 0.7 (5)	10.5 ± 3.0 (4)	44.9 ± 6.8 (7)	17.8 ± 3.2 (4)*
Smooth	10.7 ± 0.6 (6)	7.9 ± 0.9 (6)	181.7 ± 70.8 (5)	61.8 ± 12.6 (4)

A summary of mean unitary displacements and attached times for smooth and skeletal muscle myosins (± SEM) in "forward" and "reverse" populations, as well as means for independent populations of events near zero displacement. The value in parentheses indicates the number of independent data sets included in the final estimate, not the number of events. The number of events is estimated to be on the order of 10^2 for smooth muscle and 10^3 for skeletal muscle myosins.

*$p < 0.05$ between smooth and skeletal.

although negative events were very infrequent. MV histograms of force records demonstrated multiple event populations that were clearly distinguishable from baseline (Fig. 7, *right*). We observed discrete populations of force events in smooth and skeletal muscle myosins at 3.7 and 3.2 pN, respectively (Table 2), and rough multiples of these values (~7 pN). These forces were not significantly different between the two myosins. Seven-piconewton events generally occurred as a single step from baseline.

However, there was an additional population of force events near 1 pN in both myosins (Table 2). This population was absent in control experiments lacking myosin (data not shown), suggesting that they are not a system or analysis artifact. Unlike displacement MV histograms, the parameters describing baseline in force MV histograms varied significantly between experiments. Thus we were unable to accurately predetermine these parameters for force measurements. Therefore, our measurements of these "low force" populations are presented as estimates. As with displacements, measured forces will be attenuated by series compliance in the system (see Materials and Methods).

TABLE 2 Force results summary

	F (pN)		t_{on} (ms)
	High force	Low force	High force
Skeletal	3.4 ± 0.4 (4)	≈1.2 (3)	24.5 ± 6.1* (4)
Smooth	3.7 ± 0.1 (4)	≈1.5 (1)	197.5 ± 163.7 (3)

A summary of mean unitary forces and attached times for smooth and skeletal muscle myosins (± SEM) in "high force" (≈3.5 pN) and "low force" (≈1.5 pN) populations. The low-force populations are presented as estimates, as these values are heavily influenced by contributions from baseline (see text). The value in parentheses indicates the number of independent data sets included in the final estimate, not the number of events. The number of events is estimated to be on the order of 10^2 for smooth muscle and 10^3 for skeletal muscle myosins.
*$p < 0.05$ between the isometric and unloaded (forward) conditions.

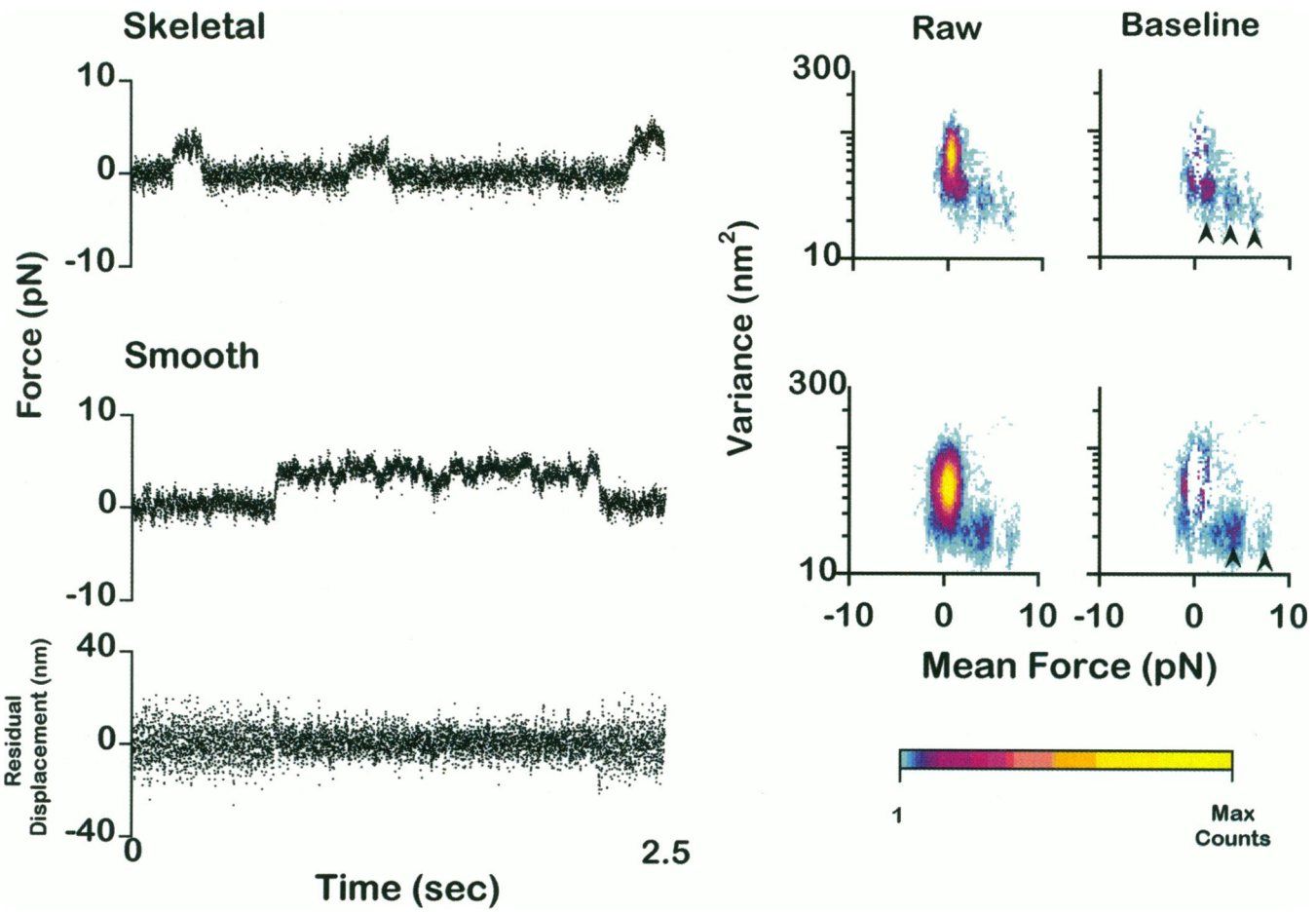

FIGURE 7 Example raw force data (*left*) and corresponding raw and baseline-subtracted MV histograms (*right*) for the entire smooth and skeletal muscle myosin data records (10 s in skeletal, 72 s in smooth; 20-ms window). The arrows indicate populations at ~1.5 (skeletal only), 3.5, and 7 pN. *Bottom trace*: Residual displacements, or those high-frequency displacements that remain during force measurements, and are used in calculating the variance in the MV histograms. Notice that the noise decreases during a force event (force trace directly above). The maximum count is 372 (149 ms) in skeletal and 1792 (717 ms) in smooth muscle myosin histograms. Parameters of fit for the two lowest forward event populations in the pictured skeletal muscle myosin histogram: population means, 0.58 and 3.53 pN; standard deviations, 0.89 and 0.59 pN; population variances, 34.7 and 26.7 nm^2; degrees of freedom, 21 and 22. Parameters of fit for the lowest forward event population in the above pictured smooth muscle myosin histogram: population mean, 3.04 pN; standard deviation, 0.67 pN; population variance, 50.9 nm^2; degrees of freedom, 18.

Smooth muscle myosin unitary force events may be longer in duration than those observed in skeletal muscle myosin, although the difference was not statistically significant because of the large spread in the smooth muscle myosin duration data. Typically, estimates of event duration vary widely between data sets, resulting in large uncertainties when these values are tallied. A similar observation has been made of on-times in fast sodium channels (Patlak and Ortiz, 1989). Our mean value for t_{on} of 24.5 ms in skeletal muscle myosin is similar to that reported for skeletal muscle HMM (Finer et al., 1994).

DISCUSSION

The objective of this study was to understand the molecular basis for the differences in mechanical performance of smooth and skeletal muscle. Therefore, the force- and motion-generating capacities for both smooth and skeletal muscle myosin were compared at the molecular level with the laser trap. Unitary force and displacement events were recorded and then analyzed using a novel mathematical transform, termed the mean-variance analysis, which was first applied to single-channel data (Patlak, 1993), and does not require the scoring of events by eye. This technique provides greater resolution in determining the existence of multiple event populations, because temporal data are transformed directly into a three-dimensional representation in mean, variance, and cumulative time. The additional resolving power that is afforded by the mean-variance histogram is analogous to that obtained when a two-dimensional gel is used to distinguish between proteins of similar molecular weight. Using this technique, we conclude that smooth and skeletal muscle myosins do not differ in their unitary force- and displacement-generating capacity, but rather in their kinetics. Mean attached times for smooth muscle myosin are longer than for skeletal muscle myosin. Differences in kinetics are thus sufficient to explain both the slower shortening velocity and enhanced force-generating capacity of smooth muscle. These kinetic differences are supported by solution biochemical studies in which the rate constants for many of the steps in the actomyosin ATPase cycle are slowed for smooth muscle myosin relative to that for skeletal muscle myosin (Marston and Taylor, 1980; Siemankowski et al., 1985). It must be noted, however, that our measurements were made at subsaturating MgATP concentrations. Therefore, any differences in K_m for MgATP between smooth and skeletal muscle myosins will affect our comparison of mean attached times. A previous study of the MgATP dependence of v_{max}, the actin filament velocity in the motility assay, shows no difference in the K_m for MgATP between smooth and skeletal muscle myosins (Warshaw et al., 1990). Furthermore, a comparison of K_m for MgATP in solution ATPase measurements showed an approximately twofold difference between smooth and skeletal muscle myosins, which was considered experimentally insignificant (Marston and Taylor, 1980). Therefore, there is no a priori reason to assume that these myosins' mechanics should have different MgATP dependencies under unloaded conditions, although we cannot unequivocally rule out some effect on attached time when significant stress exists on the cross-bridge.

Our comparisons of mean attached times are independent of any assumed distributions of force or displacement events. However, our conclusion that these myosins produce similar unitary force and displacement is based on our interpretation of the data. We argue statistically for the presence of multiple unitary event populations.

Multiple levels of displacement

We observe both "forward" and "reverse" displacements in smooth and skeletal muscle myosins, as have others in skeletal muscle HMM (Finer et al., 1994; Molloy et al., 1995a) and S-1 (Molloy et al., 1995a). Unlike previous studies, we typically discern forward and reverse displacements as distinct populations, oppositely directed but of equal magnitude. Our measured magnitudes for forward displacements were similar to those previously reported by Finer et al. (1994) for skeletal HMM, but significantly larger than those reported by Molloy et al. (1995a) for skeletal S-1. It is possible that this disparity reflects functional differences between single- and double-headed molecules (myosin/HMM versus S-1). Indeed, as Molloy et al. (1995a) point out, their data from HMM were not as well fit as those from S-1. However, different values may simply be the result of differences between laboratories in the analysis and interpretation of reverse displacements.

Molloy et al. (1995a) have proposed a model to explain the origin of reverse events. When displacement data are interpreted within the framework of this model, the true unitary displacement must be significantly smaller than the ~11 nm we observed. Briefly, Molloy et al. (1995a) assumed that the actin filament and attached microspheres undergo constrained Brownian motion described by a Gaussian distribution. This distribution is assumed to be centered on zero displacement and extends out to approximately ±30 nm, as determined by the trap stiffness. Molloy et al. assumed that the actin filament and microspheres rotate about the long axis of the filament over a period of seconds, such that binding sites are effectively available at every position along the actin filament, which is determined by the actin monomer spacing. Molloy et al. further proposed that myosin displaces the actin filament by d from wherever it happens to bind to actin during its ±30-nm excursions. Thus they predicted that the distribution of events, which were identified by a reduction in microsphere displacement variance (i.e., representing cross-bridge attachment), could be modeled by a single Gaussian, the mean of which is d and the width of which matches the distribution of actin filament positions caused by Brownian motion.

Only two of our 13 data sets were adequately fit by a single, broad distribution predicted by the model of Molloy

et al. (1995a). One might question whether MV analysis can distinguish different distributions, where many events are present at or near zero displacement. Thus, as a test of our statistical treatment and its resolving power, we generated simulated data, with a mean of 4 nm, according to the hypothesis of Molloy et al. These data were transformed into a MV histogram and processed as usual (see Fig. 8 legend for details). Despite considerable overlap with baseline, the event population was in each case adequately fit by the distribution predicted by Molloy et al. (1995a). This test demonstrates that MV analysis is able to discern, from baseline, displacements with near-zero magnitude. However, in the vast majority of cases, such a broad distribution was unable to adequately fit biological data, suggesting that multiple-event populations are a true representation of the underlying biology.

The discrete nature of our event populations may be dictated by a preferential spatial relationship between the myosin head and actin, as suggested by Huxley in 1957. Given the random nature in which the myosin adheres to the motility surface and without any knowledge of myosin's exact spatial density, it is possible that the consistent displacement values are the result of a biological bias between actin and myosin. If this is true, only those myosin molecules that are properly situated relative to actin will be selected in the laser trap experiment. If so, how could several laboratories using similar techniques obtain such different results? Two probable sources of disagreement are differences in the biology (e.g., single- versus double-headed myosins) and differences in the methods of analysis. We believe that MV analysis is the method of choice, given that scoring events by eye may lead to erroneous determinations of unitary displacement.

For example, Finer et al. (1994) identified events by eye, where "displacements smaller than or equal to the level of Brownian noise . . . were not scored." Thus, as they indicate, they likely overestimate unitary displacements. The technique used by Molloy et al. (1995a) to identify events, namely using reduced variance to guide eye scoring, suffers a different and more complex error, as follows. From looking at any of the MV histograms, it is apparent that there is a finite probability for baseline data being at low variance for a certain period of time, and this probability increases as that period of time is decreased. This is most obvious in Fig. 4 *b* and in Fig. 5, where the histogram generated with the smallest window width shows considerable low variance overlap with the event population. Therefore, if reduced variance is taken as an indication of cross-bridge attachment and an event scored as such, then one would measure many short-lived "events" near zero displacement that are, in fact, directly attributable to baseline. Thus, unless properly controlled for, any measured population of events would appear to be shifted toward baseline. This error will be particularly pronounced when the window used to calculate variance is short.

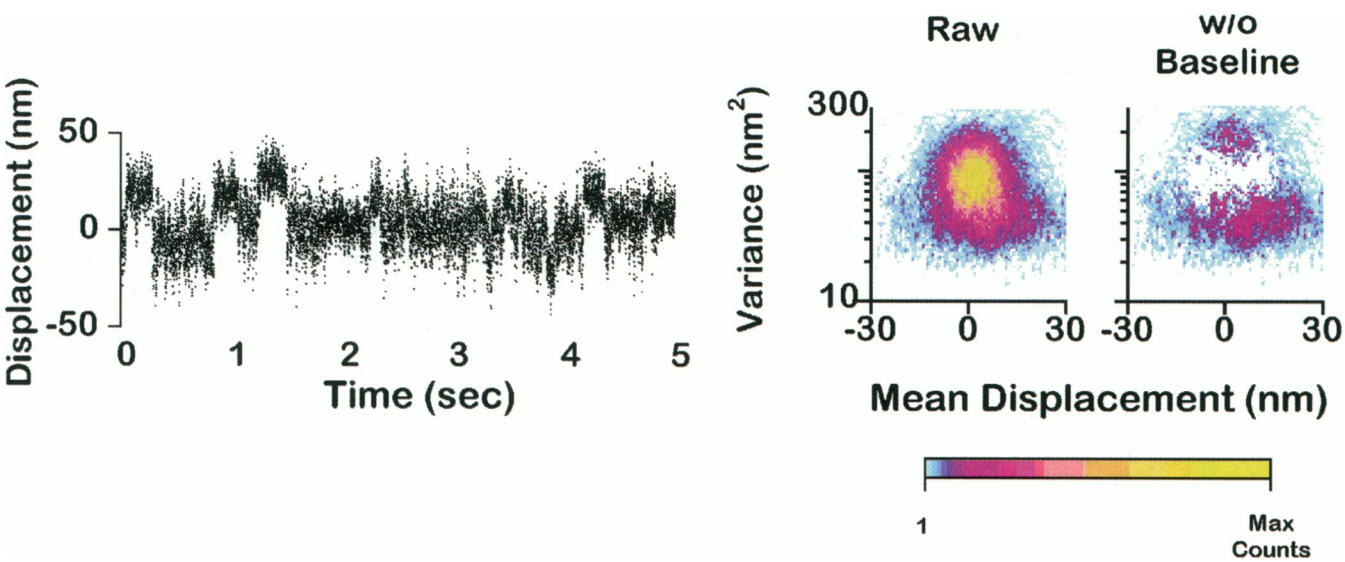

FIGURE 8 Displacement data modeled according to the hypothesis of Molloy et al. (1995b) (*left*), and corresponding raw and baseline-subtracted MV histograms (*right*) (20-ms window, 4-nm steps). Notice that a single population is observed in the MV histogram, centered on 4 nm, demonstrating the resolving power of the technique. The maximum count is 278 (111 ms). Methods: Briefly, myosin-less displacement data were recorded and assumed to represent the Brownian motion of an actin filament during an experiment. Attached (t_{on}) and detached (t_{off}) times were calculated as exponentially distributed random values (equation 25 in Patlak, 1993) based on a duty cycle of 20–40% and a mean attached time of 90 ms (Molloy et al., 1995b). First, a segment of data representing baseline was written unchanged to the output file. Next, a segment of data representing events was modified as follows: (*a*) the noise was reduced by 30% to simulate myosin attachment, and (*b*) the measured step size was calculated as the sum of the actual step size (4 nm) and the position of the microsphere at the beginning of the step. This value was added to the reduced noise, and the data were written to the output file. Events modeled in this fashion were confirmed to be distributed as predicted by the model of Molloy et al. (1995b). This cycle of calculating pseudorandom durations and writing baseline and event segments was repeated as needed to give data sets 60 s in duration. A 30% drop in noise during events was confirmed experimentally.

The model proposed by Molloy et al. (1995a) is both simple and elegant. However, based on our analysis, we believe the actual physical properties of the system to be more complex, as the bulk of our data are consistent with discrete forward and reverse displacement populations. Our data do not refute the 4-nm estimate predicted by Molloy et al. (1995a) for skeletal S-1. In fact, it is possible that rapid, cooperative movement of paired myosin heads, each producing ~4–6 nm of displacement, would explain the 11-nm steps we observe for both smooth and skeletal muscle myosin. Indeed, although Molloy and co-workers' (1995a) displacement data for myosin S-1 were well fit by a broad histogram centered near 4 nm, their displacement data for HMM were not as well fit. It is possible that the presence of a second head is required for HMM or myosin to achieve a full working stroke of ~11 nm (Block, 1995). It is tempting to speculate that in cases in which we observed a single, broad population centered near 6 nm, that one head of myosin was "stuck" to the motility surface, rendering that particular molecule single-headed. Alternatively, the 4-nm estimate for S-1 may reflect a compromise in the subfragment's function. Even at saturating concentrations, skeletal S-1 produces considerably slower v_{max} compared to HMM or whole myosin (Toyoshima et al., 1987).

The origin of reverse events is still of considerable interest, and they may be explained by several models. First, in addition to the simple "Brownian motion capture" explanation proposed by Molloy et al. (1995a), Molloy et al. (1995b) also proposed the attachment of myosin during its repriming phase, thus resulting in a work-stroke reversal. Second, it is possible that reverse events arise from improperly oriented myosin heads that have swiveled 180°, allowing them to attach to actin in a stereo-specific manner. The reverse event might then occur as the myosin attempts to relieve the strain in the molecule. Third, myosin may move processively as a two-headed molecule to produce its full range of motion in a mechanism proposed for kinesin (Peskin and Oster, 1995). Forward or reverse steps might then occur as the free head attaches ±11 nm, or two binding sites forward or backward, respectively. Finally, myosin may work as a "thermal ratchet," where ±11 nm again corresponds to the attachment of myosin two binding sites forward or backward. However, let us assume that the conformational changes that produce d under unloaded conditions also occur and produce F under "isometric" conditions. The work one then calculates for whole myosin, $\sim\frac{1}{2}F{\cdot}d$ (~8–19 pnJ), or S-1 (~3.5 pnJ; Molloy et al., 1995a) exceeds the available translational energy, $\frac{1}{2}k_BT$ (2.05 pnJ at 298 K). Thus a pure thermal ratchet model seems unlikely.

We should also note that, given our "unloaded" experimental conditions, myosin experiences a load of ~0.88 pN, based on a dual trap stiffness of 0.08 pN/nm and an 11-nm step. This load is about 25% of myosin's unitary force of 3.5 pN (see below). Thus our measured unitary displacement of 11 nm could be an underestimate. If we assume a linear force-displacement relationship for myosin, as has been measured in skeletal HMM (Finer et al., 1995), one would predict a zero-load unitary displacement of ~14.7 nm for both myosins. In addition, the points of attachment of the actin filament to the microspheres introduce a series compliance that is a highly nonlinear function of preload (Dupuis et al., 1997). This compliance, and the internal compliance of myosin, may cause further underestimates of d and F.

Multiple levels of force

Finer et al. (1994) and Molloy et al. (1995a) reported average unitary forces of 3.5 pN and 1.7 pN, respectively, in skeletal HMM. We observed populations in our data corresponding roughly to each of these values, and higher populations did not appear to be the result of multiple events (i.e. "staircases"). Which population represents the "true" unitary force is unknown and depends on the functional origin of each population. However, because each of these populations exists in both smooth and skeletal muscle myosins, we must conclude that these myosins' unitary forces are similar.

Several explanations are apparent for the multiple force populations. First, 1.2–1.5-pN events might be due to myosins that are not optimally aligned to generate force (Ishijima et al., 1994). Second, 1.2–1.5-pN events may be due to a single head, whereas 3.5- and 7.0-pN events result from two and four heads, respectively. The absence of a ~5-pN event population (representing three heads) leads us to doubt this. Nonetheless, one might envision that the two heads in smooth muscle myosin are more positively cooperative than in skeletal muscle myosin. Unlike skeletal muscle myosin, adjacent heads of smooth muscle HMM bound in rigor may be cross-linked (Onishi et al., 1990). Furthermore, cross-linking the heads of smooth muscle myosin increases their association constant with actin (Onishi and Fujiwara, 1990). These data suggest that the two heads of smooth muscle myosin may interact in some subtle cooperative fashion. Measurements of unitary force and unitary displacement in single-headed smooth and skeletal muscle myosins may resolve this issue.

A final explanation for multiple force populations is that the different levels of force represent different states in the cross-bridge cycle (Kawai and Zhao, 1993). For example, Brenner et al. (1995) proposed that a conformational change during the weak-strong binding transition is responsible for the production of isometric force, whereas subsequent conformational changes are responsible for quick tension recovery. Therefore, the 1.2–1.5-pN events may reflect the force generated by a conformational change upon strong binding, whereas the ~3.5-pN events reflect additional, larger conformational changes, or vice versa. If the different levels of force do indeed represent different states in the cross-bridge cycle, one should be able to cause these populations to redistribute by adding hydrolysis products (i.e., PP_i, ADP) to the motility solution, or by altering the ionic strength (weak versus strong binding).

Mechanical differences between myosins

Our data at the molecular level help to explain smooth muscle myosin's enhanced average force-generating capacity, and slower actin filament velocity, compared to skeletal muscle myosin. To understand how one myosin might produce a velocity or force different from that of another, consider this simple two-state model of the myosin cross-bridge cycle:

$$\text{Weak} \underset{1/t_{on}}{\overset{1/t_{off}}{\rightleftharpoons}} \text{Strong}, \tag{8}$$

where t_{on} is the mean time myosin spends in the strongly bound state and t_{off} is the mean time myosin spends in the weakly bound state. In this model, when a cross-bridge undergoes a transition from the weakly bound to the strongly bound state, a working stroke occurs that generates a displacement d (the "unitary displacement") under unloaded conditions, or a force F (the "unitary force") under maximally loaded conditions. This is a reasonable model for the mechanics of the system, provided that the working stroke occurs simultaneously with, or rapidly after, transition to the strongly bound state. Another important aspect of this model is that the transition rates between states are load dependent (Huxley, 1957). Therefore, any consideration of myosin's transition rates must be qualified by indicating the load that exists on the actomyosin system.

In the motility assay under unloaded conditions, actin filaments will be driven by a population of myosin molecules at a maximum velocity, v_{max}. It is assumed that at any point in time at least one myosin head is strongly bound to the actin filament and undergoing its working stroke. Thus, at the molecular level, v_{max} should be related to d and the unloaded t_{on} (Huxley, 1990):

$$v_{max} \approx d/t_{on}. \tag{9}$$

Based on our molecular measurements, smooth muscle's slower unloaded shortening velocity must be due in part to its longer t_{on} than skeletal muscle myosin, because d is similar for these two myosin types.

We have previously shown that smooth muscle myosin's time-averaged force, F_{avg}, produced under maximally loaded, isometric conditions is 3–4 times greater than that of skeletal muscle myosin (Harris et al., 1994; VanBuren et al., 1994b). Once again, assuming this simple two-state model, F_{avg} can be defined by the following equation:

$$F_{avg} = F \cdot f, \tag{10}$$

where f is the isometric duty cycle, or the fraction of the total cycle time spent producing the unitary force, F. Because smooth and skeletal muscle myosins exhibit similar unitary forces based on our measurements, the greater F_{avg} produced by smooth muscle myosin must, by elimination, be the result of a greater isometric duty cycle. This hypothesis is supported by conclusions drawn from mechanical experiments on single isolated smooth muscle cells (Warshaw and Fay, 1983; Warshaw, 1987; Yamakawa et al., 1990).

It may be possible to estimate the isometric duty cycle for smooth and skeletal muscle myosin based on previous F_{avg} measurements of 0.6 pN for smooth and 0.2 pN for skeletal muscle myosin (VanBuren et al., 1994b). If we assume that these myosins produce a similar F of 3.5 pN, then the isometric duty cycles for smooth and skeletal muscle myosins will be 17% and 6%, respectively. However, we believe that F_{avg} values are most likely an underestimate by at least a factor of 2–3, because these measurements were made using randomly oriented, monomeric myosin on the motility surface. This correction may translate into isometric duty cycles that may be as high as 51% and 18% for smooth and skeletal muscle myosins, respectively.

Molecular basis for differences in mechanical performance

Given the skeletal myosin S-1 crystal structure (Rayment et al., 1993), is it possible to identify the structural domains that contribute to the functional differences between smooth and skeletal muscle myosin? The S-1 structure is characterized as an asymmetrical molecule containing a large globular motor domain from which projects an 85-Å-long α-helical "neck" to which the essential and regulatory light chains are bound. This neck region may act as a lever arm to amplify and transmit small conformational changes that originate within the motor domain (Rayment et al., 1993; VanBuren et al., 1994a; Uyeda et al., 1996; Guilford et al., 1996). Because we observed no differences in unitary displacement or force, it seems unlikely that gross differences in length exist for the neck region of these two myosins. However, differences in kinetics (i.e., t_{on}) were observed, suggesting that structural domains governing the kinetics of the cycle are likely candidates.

One approach to identifying structurally sensitive domains is to use naturally occurring myosins that have slight differences in their primary amino acid sequence but substantially different enzymatic and motor properties. For example, there are two smooth muscle myosin isoforms that are the products of alternative splicing of a 7-amino acid insert at the 25/50-kDa junction (White et al., 1993; Barbij et al., 1991). These myosins have significantly different hydrolytic and mechanical capacities, supporting the importance of this domain to the kinetics of the motor. In fact, Spudich (1994) suggested that a surface loop at this junction, which presumably bridges the opening to the nucleotide pocket, may govern the rate of ADP release after the power stroke. In addition, he proposed that the actin binding loop that bridges the 50- and 20-kDa proteolytic fragments near the actin-binding site controls the weak to strong binding transition, which is rate-limiting for ATP hydrolysis (Spudich, 1994). However, recent data from chimeric smooth muscle HMM suggest that this may not be a universal mechanism (Rovner et al., 1996). The next step will

be to judiciously engineer a chimera that can be studied in the laser trap, in the hope of unraveling the mystery of smooth muscle myosin's unique mechanical capabilities.

The authors wish to acknowledge the following persons for their invaluable contributions to this study: Eric Hayes for protein isolations and experimental preparations; Bill Stuono for computer programming; Taka Ashikaga of the University of Vermont Biometrics Department for his statistics expertise; the University of Vermont Muscle Club and Kathleen Trybus for discussions and helpful suggestions all along the way; Justin Molloy for commiserating during the development of the trap; and Steven Block for assistance during the early design of the instrumentation. The authors also gratefully acknowledge the reviewers and editor of this manuscript, for it is much improved because of their efforts.

This work was supported by grants from the National Institutes of Health to WHG (HL08932) and to DMW (AR42231).

Software packages for mean-variance analysis will soon be publicly available. Contact Drs. Patlak (patlak@salus.med.uvm.edu) or Guilford (guilford@salus.med.uvm.edu) for additional information.

REFERENCES

Ashkin, A., J. M. Dziedzic, J. E. Bjorkholm, and S. Chu. 1986. Observation of a single-beam gradient force optical trap for dielectric particles. *Opt. Lett.* 11:288–290.

Barbij, P., C. Kelly, and M. Periasamy. 1991. Characterization of a mammalian smooth muscle myosin heavy-chain gene: complete nucleotide and protein coding sequence and analysis of the 5′ end of the gene. *Proc. Natl. Acad. Sci. USA.* 88:10676–10680.

Block, S. M. 1995. One small step for myosin. *Nature.* 378:132–133.

Block, S. M., and K. Svoboda. 1995. Analysis of high resolution recordings of motor movement. *Biophys. J.* 68:230s–241s.

Brenner, B., J. M. Chalovich, and L. C. Yu. 1995. Distinct molecular processes associated with isometric force generation and rapid tension recovery after quick release. *Biophys. J* 68:106s–11s.

Dupuis, D. E., W. H. Guilford, J. Wu, and D. M. Warshaw. 1997. Actin filament mechanics in the laser trap. *J. Muscle Res. Cell Motil.* (in press).

Fay, F. S., D. D. Rees, and D. M. Warshaw. 1981. The contractile mechanism in smooth muscle. *In* Membrane Structure and Function, Vol. 4. E. E. Bitter, editor. Wiley and Sons, New York. 80–130.

Finer, J. T., A. D. Mehta, and J. A. Spudich. 1995. Characterization of single actin-myosin interactions. *Biophys. J.* 68:291s–97s.

Finer, J. T., R. M. Simmons, and J. A. Spudich. 1994. Single myosin molecule mechanics: piconewton forces and nanometer steps. *Nature.* 368:113–119.

Guilford, W. H., M. J. Tyska, Y. Freyzon, D. M. Warshaw, and K. M. Trybus. 1996. Smooth muscle myosin with an elongated neck region produces greater unitary displacements in vitro. *Biophys J.* 70(2, part 2):A127.

Harada, Y., A. Noguchi, A. Kishino, and T. Yanarida. 1987. Sliding movement of single actin filaments on one-headed myosin filaments. *Nature.* 326:805–808.

Harris, D. E., and D. M. Warshaw. 1993a. Smooth and skeletal muscle myosin both exhibit low duty cycles at zero load in vitro. *J. Biol. Chem.* 268:14764–14768.

Harris, D. E., and D. M. Warshaw. 1993b. Smooth and skeletal muscle actin are mechanically indistinguishable in the in vitro motility assay. *Circ. Res.* 72:219–224.

Harris, D. E., S. S. Work, R. K. Wright, N. R. Alpert, and D. M. Warshaw. 1994. Smooth, cardiac and skeletal muscle myosin force and motion generation assessed by cross-bridge mechanical interactions in vitro. *J. Muscle Res. Cell Motil.* 15:11–19.

Huxley, A. F. 1957. Muscle structure and theories of contraction. *Prog. Biophys.* 7:255–317.

Huxley, H. E. 1990. Sliding filaments and molecular motile systems. *J. Biol. Chem.* 265:8347–8350.

Ishijima, A., Y. Harada, H. Kojima, T. Funatsu, H. Higuchi, and T. Yanagida. 1994. Single-molecule analysis of the actomyosin motor using nano-manipulation. *Biochem. Biophys. Res. Commun.* 199: 1057–1063.

Kawai, M., and Y. Zhao. 1993. Cross-bridge scheme and force per cross-bridge state in skinned rabbit psoas muscle fibers. *Biophys. J.* 65: 638–651.

Kron, S. J., and J. A. Spudich. 1986. Fluorescent actin filaments move on myosin fixed to a glass surface. *Proc. Natl. Acad. Sci. USA.* 83: 6272–6276.

Marston, S. B., and E. W. Taylor. 1980. Comparison of the myosin and actomyosin ATPase mechanisms of the four types of vertebrate muscles. *J. Mol. Biol.* 139:573–600.

Miyata, H., H. Hakozaki, H. Yoshikawa, N. Suzuki, K. Kinosita, Jr., T. Naishizaka, and S. Ishiwata. 1994. Stepwise motion of an actin filament over a small number of heavy meromyosin molecules is revealed in an in vitro motility assay. *J. Biochem.* 115:644–647.

Molloy, J. E., J. E. Burns, J. Kendrick-Jones, R. T. Tregear, and D. C. S. White. 1995a. Movement and force produced by a single myosin head. *Nature.* 378:209–212.

Molloy, J. E., J. E. Burns, J. C. Sparrow, R. T. Tregear, J. Kendrick-Jones, and D. C. S. White. 1995b. single-molecule mechanics of heavy meromyosin and s1 interacting with rabbit or *Drosophila* actins using optical tweezers. *Biophys. J.* 68:298s–305s.

Murphy, R. A., J. T. Herlihy, and J. Megerman. 1974. Force-generating capacity and contractile protein content of arterial smooth muscle. *J. Gen. Physiol.* 64:691–705.

Onishi, H., and K. Fujiwara. 1990. The rigor configuration of smooth muscle heavy meromyosin trapped by a zero-length cross-linker. *Biochemistry.* 29:3013–3023.

Onishi, H., T. Maita, G. Matsuda, and K. Fujiwara. 1990. Lys-65 and Glu-168 are the residues for carbodiimide-catalyzed cross-linking between the two heads of rigor smooth muscle heavy meromyosin. *J. Biol. Chem.* 265:19362–19368.

Pardee, J. D., and J. A. Spudich. 1982. Purification of muscle actin. *Methods Enzymol.* 85:164–81.

Patlak, J. B. 1993. Measuring kinetics of complex single ion channel data using mean-variance histograms. *Biophys. J.* 65:29–42.

Patlak, J. B., and M. Ortiz. 1989. Kinetic diversity of Na^+ channel bursts in frog skeletal muscle. *J. Gen. Physiol.* 94:279–301.

Peskin, C. S., and G. Oster. 1995. Coordinated hydrolysis explains the mechanical behavior of kinesin. *Biophys. J.* 68:202s–211s.

Press, W. H., B. P. Flannery, S. A. Teukolsky, and W. T. Vetterling. 1988. Numerical Recipes. Cambridge University Press, New York.

Rayment, I., W. R. Rypniewski, K. Schmidt-Base, R. Smith, D. R. Tomchick, M. M. Benning, D. A. Winkelmann, G. Wesenberg, and H. M. Holden. 1993. Three-dimensional structure of myosin subfragment-1: a molecular motor. *Science.* 261:50–58.

Rovner, A. S., Y. Freyzon, and K. M. Trybus. 1996. Chimeric substitutions of the actin binding loop disrupt regulation of smooth muscle heavy meromyosin. *J. Biol. Chem.* 270:30260–302263.

Siemankowski, R. F., M. O. Wiseman, and H. D. White. 1985. ADP dissociation from actomyosin subfragment 1 is sufficiently slow to limit the unloaded shortening velocity in vertebrate muscle. *Proc. Natl. Acad. Sci. USA.* 82:658–662.

Simmons, R. M., J. T. Finer, S. Chu, and J. A. Spudich. 1996. Quantitative measurements of force and displacement using an optical trap. *Biophys. J.* 70:1813–1822.

Skoog, D. A., and D. M. West. 1982. Fundamentals of Analytical Chemistry, 4th Ed. Sauders College Publishing, New York.

Spudich, J. A. 1994. How molecular motors work. *Nature.* 372:515–518.

Svoboda, K., and S. M. Block. 1994. Biological applications of optical forces. *Annu. Rev. Biophys. Biomol. Struct.* 23:247–285.

Toyoshima, Y. Y., S. J. Kron, E. M. McNally, K. R. Niebling, C. Toyoshima, and J. A. Spudich. 1987. Myosin subfragment-1 is sufficient to move actin filaments in vitro. *Nature.* 328:536–539.

Uyeda, T. Q., P. D. Abramson, and J. A. Spudich. 1996. The neck region of the myosin motor domain acts as a a lever arm to generate movement. *Proc. Natl. Acad. Sci. USA.* 93:4459–4464.

VanBuren, P., G. S. Waller, D. E. Harris, K. M. Trybus, D. M. Warshaw, and S. Lowey. 1994a. The essential light chain is required for full force production by skeletal muscle myosin. *Proc. Natl. Acad. Sci. USA.* 91:12403–12407.

VanBuren, P., S. S. Work, and D. M. Warshaw. 1994b. Enhanced force generation by smooth muscle myosin in vitro. *Proc. Natl. Acad. Sci. USA.* 91:202–205.

Warshaw, D. M. 1987. Force:velocity relationship in single isolated toad stomach smooth muscle cells. *J. Gen. Physiol.* 89:771–789.

Warshaw, D. M., J. M. Desrosiers, S. S. Work, and K. M. Trybus. 1990. Smooth muscle myosin cross-bridge interactions modulate actin filament sliding velocity in vitro. *J. Cell Biol.* 111:453–463.

Warshaw, D. M., and F. S. Fay. 1983. Cross-bridge elasticity in single smooth muscle cells. *J. Gen. Physiol.* 82:157–199.

White, S., A. F. Martin, and M. Periasamy. 1993. Identification of a novel smooth muscle myosin heavy chain cDNA: isoform diversity in the S1 head region. *Am. J. Physiol.* 264(5, Pt 1):C1252–C1258.

Yamakawa, M., D. E. Harris, F. S. Fay, and D. M. Warshaw. 1990. Mechanical transients of single toad stomach smooth muscle cells. *J. Gen. Physiol.* 95:697–715.